

# Processing SAR data of rugged terrain by time-domain back-projection

Othmar Frey and Erich H. Meier and Daniel R. Nüesch

Remote Sensing Laboratories, University of Zurich, CH-8057 Zurich, Switzerland

## ABSTRACT

Processing of SAR images of rugged terrain deserves special care because the topography affects the focused image in a number of ways. In order to obtain geometrically and radiometrically corrected SAR images of mountainous areas additional knowledge about the topography and the sensor's trajectory and attitude has to be included in the processing or post-processing steps. Various well-known focusing techniques are available to transform SAR raw data into a single look complex image such as the range-Doppler, the chirp scaling or the  $\omega$ -k algorithm. While these algorithms perform the azimuth focusing step in the frequency domain the time-domain back-projection processing technique focuses the data geometrically, i.e., in the time domain.

In contrast to the frequency-domain techniques, time-domain back-projection maintains the entire geometric relationship between the sensor and the illuminated area. This implies a couple of advantages: a stringent, terrain-based correction for the elevation antenna gain pattern may be implemented and topography-induced variation of radar brightness can be eliminated in a single step. Further, the SAR image is focused directly onto an arbitrary reconstruction grid and in the desired geodetic reference frame without requiring any additional processing steps.

We discuss the influence of rugged terrain on the radiometric properties of focused SAR data and demonstrate how the time-domain back-projection approach accounts for these effects within one integrated processing framework by incorporating both a correction for terrain slope induced variation of radar brightness and a stringent correction for the elevation antenna gain pattern. The algorithm is evaluated for ENVISAT/ASAR image mode data of a mountainous area.

**Keywords:** SAR processing, back-projection, radiometric correction, antenna gain pattern correction, geocoding, topography, digital elevation model, Envisat, ASAR.

## 1. INTRODUCTION

This work is motivated by taking the point of view of an end-user who, in order to be able to retrieve bio- or geophysical parameters, is interested in SAR data that is not only well focused, but also geographically referenced as well as accurate in terms of geolocation and radiometry.

Topography causes geometric and radiometric distortions in the SAR image deteriorating its interpretability considerably. While geocoding and radiometric correction of SAR data is rather straightforward for flat terrain these two (post-)processing steps deserve special care when dealing with images of rugged terrain. In order to obtain geometrically and radiometrically corrected SAR images of mountainous areas additional knowledge about the topography and the sensor's trajectory and attitude has to be included in the processing or post-processing steps.

Various azimuth focusing techniques are available to transform SAR raw data to a single look complex (SLC) image such as the range-Doppler (RD) [1], the chirp scaling (CS) [2] [3] and the  $\omega$ -k [4] algorithm. An up-to-date overview and comparison of these algorithms is given in [5]. While these algorithms focus the SAR data in the

---

Copyright 2005 Society of Photo-Optical Instrumentation Engineers.

This paper was published in "Proceedings of SPIE Vol. 5980: SAR Image Analysis, Modeling and Techniques X" and is made available as an electronic reprint with permission of SPIE. One print or electronic copy may be made for personal use only. Systematic or multiple reproduction, distribution to multiple locations via electronic or other means, duplication of any material in this paper for a fee or for commercial purposes, or modification of the content of the paper are prohibited.

one- or two-dimensional frequency domain the also well-known time-domain back-projection (TDBP) processing technique [6] [7] applies a completely different approach: as the name says the SAR data are focused in the time domain, which is equivalent to saying that they are focused geometrically.

Time-domain back-projection, due to its geometric nature, provides a framework to incorporate geocoding and radiometric correction within the azimuth focusing step. Therefore it has the potential to provide an accurate reconstruction of SAR data of rugged terrain also in terms of radiometric fidelity. In [8] it has been demonstrated for ENVISAT/ASAR image mode (IM) data of transponders and a corner reflector that both the radiometric performance and the geolocation accuracy achieved by TDBP processing, are equivalent to the quality parameters obtained when using a RD processor [9]. Due to its geometric nature TDBP develops its potential when processing SAR data of rugged terrain.

First, correction approaches for elevation angle dependent antenna gain and methods to correct for topography-induced variation of radar brightness are briefly revised. Then, the system model of TDBP processing is presented. Finally, the algorithm is evaluated with the help of ENVISAT/ASAR IM data of a mountainous region.

## 2. ELEVATION ANTENNA GAIN PATTERN CORRECTION

A common approach to correct for the variation of the elevation antenna gain pattern uses a slant-range dependent elevation (also: off-nadir) angle estimate based on a simple ellipsoid model at a mean reference height [10]. However, this approximation is only valid in case of flat terrain because the elevation angle corresponding to a specific position within the radar swath is a function of both slant-range distance *and* altitude of that position. In rugged terrain, situations may occur where two backscatterers exhibit the same range distance although the elevation angles, under which they are seen by the sensor, differ completely.

Considering the TerraSAR-X system as example it has been shown theoretically [11] that, depending on the imaged swath, radiometric errors rapidly exceed 1 dB for unaccounted altitude differences of 500 - 1500 m between the actual terrain and the reference height. Errors are most prominent for swaths at small off-nadir angles and at the edges of the beam where the absolute slope of the antenna gain pattern increases. Using antenna gain patterns for ENVISAT/ASAR IM data of alpine regions radiometric errors exceeding 3 dB were reported in [12] when applying the approximative correction.

A stringent antenna gain pattern correction requires knowledge about the geometric constellation between each backscatterer and the sensor. With the help of a digital terrain model the correct elevation angle information for each pixel can be provided. In case of TDBP processing the exact elevation angle can even be calculated for each sensor and target position. However, the radiometric errors introduced by an inappropriate correction for the antenna gain pattern are, although significant, still exceeded by topography-induced variation of radar brightness [12].

## 3. VARIATION OF RADAR BRIGHTNESS DUE TO TOPOGRAPHY

SAR images of rugged terrain basically exhibit two effects caused by surface slopes. One effect is the variation of radar brightness and the second is a change of the polarization orientation induced by azimuth slopes [13]. The focus of this paper is laid on the first effect, the latter is not considered further here.

Ulander [14] showed that two widely used methods, one based on local incidence angle and the second based on surface tilt angles, are only approximative slope corrections and proposed a more accurate correction scheme in terms of a projection cosine:

$$\sigma^0 = \beta^0 \cos \psi , \quad (1)$$

where  $\sigma^0$  is the backscatter coefficient, which is defined as the average radar cross section per unit ground area,  $\beta^0$  is the radar brightness, which is defined as the average radar cross section per unit image area, and where  $\psi$  is the projection angle, which relates the unit image area to the unit ground area.  $\psi$  is the angle between the image plane normal and the surface normal, hence, it is complementary to the smallest angle between the surface normal and the image plane [14]. A drawback of this method is that it assumes that a ground element is uniquely related to an image element and therefore does not consider layover and shadowing regions. It is

also required that the image coordinate system be orthogonal, an assumption which is justifiable for spaceborne stripmap SAR but which is not satisfied in general.

A more stringent formulation of the variation of radar brightness within SAR images has been proposed in [15] taking into account the non-homomorphic nature of the relationship between the SAR image and the map projection.

Currently, we use the projection cosine approach in our experimental TDBP processor and therefore we restrict ourselves to this method throughout this paper. Originally this method had been used for radiometric calibration of SLC images. Its adaptation to TDBP is straightforward as will be shown in the next section.

#### 4. SYSTEM MODEL

We briefly revise the system model of TDBP processing as described in [6] and rewrite it as a function of the three-dimensional position of a point in the reconstruction grid, which is the convenient form for our purpose. Reference [6] gives a comprehensive overview of TDBP and of fast back-projection techniques, which make use of approximations in order to reduce the computational burden. Another source which extensively discusses the subject is [7].

Assuming a linear sensor path the two-way response  $g$  for a single point target can be written as a function of the cylinder coordinates  $(\rho, \theta, x)$  where  $\rho$  is the range distance at the point of closest approach between sensor and target,  $\theta$  is the elevation angle, and  $x$  is the azimuth position along the linear flight path:

$$g(R, x) = A(\cdot) \cdot \sigma_0 \cdot \frac{p_{rc}(R - \sqrt{(x - x_0)^2 + \rho_0^2})}{(x - x_0)^2 + \rho_0^2}. \quad (2)$$

$R$  is the range distance,  $A(\cdot)$  the amplitude function representing the antenna gain pattern,  $\sigma_0$  the reflectivity of the point target at position  $(\rho_0, \theta_0, x_0)$ , and  $p_{rc}$  is the demodulated, range-compressed pulse.

The focused SAR signal  $s$  after TDBP at the range/azimuth position  $(\rho, x)$  is:

$$s(\rho, x) = \sum_{x'} g(R, x) \cdot R \cdot \exp(j2k_c R), \quad (3)$$

where  $R = \sqrt{(x' - x)^2 + \rho^2}$  is the range distance,  $x'$  the along-track integration parameter,  $k_c = 2\pi f_c/c$  the central wavenumber corresponding to the carrier frequency  $f_c$ , and  $c$  is the speed of light. The exponential term brings the demodulated signal back to its original bandpass form.

Generalising to an arbitrary sensor path the two-way response  $g$  for a single point target at position  $\vec{r}_0$  can be written as:

$$g(R, \vec{r}_S) = A(\vec{r}_S, \vec{r}_0) \cdot \sigma_0 \cdot \frac{p_{rc}(R - |\vec{r}_S - \vec{r}_0|)}{|\vec{r}_S - \vec{r}_0|^2}, \quad (4)$$

where  $A(\vec{r}_S, \vec{r}_0)$  is the amplitude function representing the antenna gain pattern,  $\sigma_0$  the reflectivity of the point target at position  $\vec{r}_0$ ,  $p_{rc}$  the demodulated and range-compressed pulse,  $\vec{r}_S$  the three-dimensional position vector of the sensor, and  $R$  the range distance.

In order to be able to back-project the data directly to a three-dimensional reconstruction grid consisting of the grid points  $\vec{r}_i$  we want to express the back-projected signal  $s$  not as a function of the range position  $\rho$  and the sensor position  $\vec{r}_S$ , but as a function of the grid point  $\vec{r}_i$ :

$$s(\vec{r}_i) = \sum_{j=a(\vec{r}_i)}^{b(\vec{r}_i)} g(|\vec{r}_i - \vec{r}_{S_j}|, \vec{r}_{S_j}) \cdot |\vec{r}_i - \vec{r}_{S_j}| \cdot \exp(j2k_c |\vec{r}_i - \vec{r}_{S_j}|), \quad (5)$$

where  $a$  and  $b$  are the indices of the first and last sensor position, respectively, the echo of which still contributes to the grid position  $\vec{r}_i$ . This means that we sum up the contributions from those sensor positions  $\vec{r}_{S_j}$  which

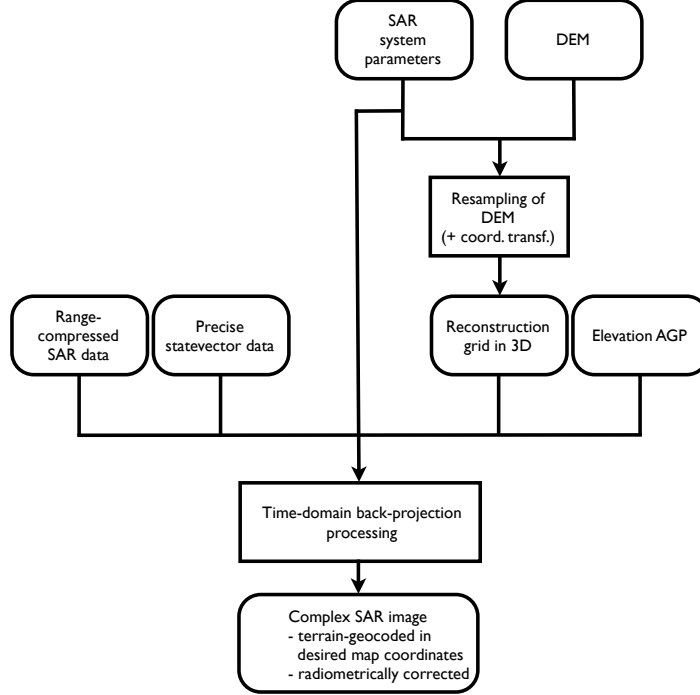


**Figure 1.** Flow diagram of the integrated processing and geocoding approach using time-domain back-projection.

build the synthetic aperture for the grid position  $\vec{r}_i$ . Note that  $a$  and  $b$  vary as a function of the grid position  $\vec{r}_i$ . Introducing the projection cosine term, which is a function of the projection angle  $\psi(\vec{r}_i, \vec{r}_{S_j})$ , yields:

$$s(\vec{r}_i) = \sum_{j=a(\vec{r}_i)}^{b(\vec{r}_i)} \cos(\psi(\vec{r}_i, \vec{r}_{S_j})) \cdot g(|\vec{r}_i - \vec{r}_{S_j}|, \vec{r}_{S_j}) \cdot |\vec{r}_i - \vec{r}_{S_j}| \cdot \exp(j2k_c|\vec{r}_i - \vec{r}_{S_j}|). \quad (6)$$

Equation (6) builds the basis of the TDBP algorithm as it is applied to the data presented in this paper. Since the actual signal is sampled at discrete points in time an appropriate interpolation procedure has to be implemented in order to retrieve the range-compressed data at the correct range distances. Fig. 1 depicts the processing chain of integrated azimuth-focusing and geocoding by means of TDBP.

## 5. DATA

The effectiveness of the discussed approach will be demonstrated using an ENVISAT/ASAR scene of a mountainous area in central Switzerland. The C-band data has been acquired in image mode (IM) during a descending pass on orbit 7963 at beam IS6, which has a central off-nadir angle of  $35.6^\circ$ . The scene depicts a  $10 \text{ km} \times 10 \text{ km}$  area around Rigi Mountain situated between the Lake Zug and Lake Lucerne. Altitudes range from 413 m on the surface of Lake Zug up to 1797 m at the top of Rigi Mountain. The terrain features strong variations of slope angles with respect to both range and azimuth direction of the scene.

The three steps, azimuth focusing, geocoding, and radiometric correction have been performed simultaneously using our integrated processing algorithm based on TDBP. Both, range and azimuth spectra have been windowed by a Hamming window with a coefficient of 0.75. Further, a fraction of 80% of the total Doppler bandwidth has been processed.

As the data are processed they are resampled to a reconstruction grid in local map coordinates with a sample spacing of 3.125 m. The grid is derived from a 25 m - spaced digital elevation model (DEM) by cubic spline interpolation. A prerequisite for accurate geolocation without ground control points is, besides an accurate DEM,

the availability of precise sensor positioning data, which is given for ENVISAT/ASAR. ENVISAT/DORIS precise orbit data (DOR\_VOR\_AX) build the source for accurate sensor positioning. State vectors are provided at intervals of 60 s. According to [16] the total absolute orbit error is as low as 10 cm RMS and the absolute radial error even lower than 5 cm RMS. Interpolating the intermediate state vectors using a higher-order polynomial certainly deteriorates the accuracy, but the errors are expected to remain small compared to the resolution capabilities of the ASAR system or the accuracy of a DEM. In addition, ENVISAT/ASAR elevation antenna gain pattern data provided in external calibration files (XCA) are used in order to perform a stringent, DEM-based correction for the elevation antenna gain pattern.

## 6. EXPERIMENTAL RESULTS

The presented TDBP algorithm for simultaneous azimuth focusing, geocoding and radiometric correction has been tested using ENVISAT/ASAR IM data and auxiliary data described above. Fig. 2(a) depicts the focused and geocoded data processed by TDBP in local map coordinates, but without radiometric corrections. Strong variations of the backscatter coefficients due to rugged terrain are a dominating feature. In Fig. 2(b) the radiometrically corrected image is shown. The radiometric adjustment consists of both a correction for variation of radar brightness based on a projection cosine term and a stringent, DEM-based elevation antenna gain pattern correction. In regions where layover occurs the applied radiometric correction approach is not valid. Therefore, layover regions (Fig. 3(a)) are segregated and build, together with the areas of radar shadow (Fig. 3(b)), a mask, which is superimposed on the corrected SAR image. At each sensor position the slope correction and

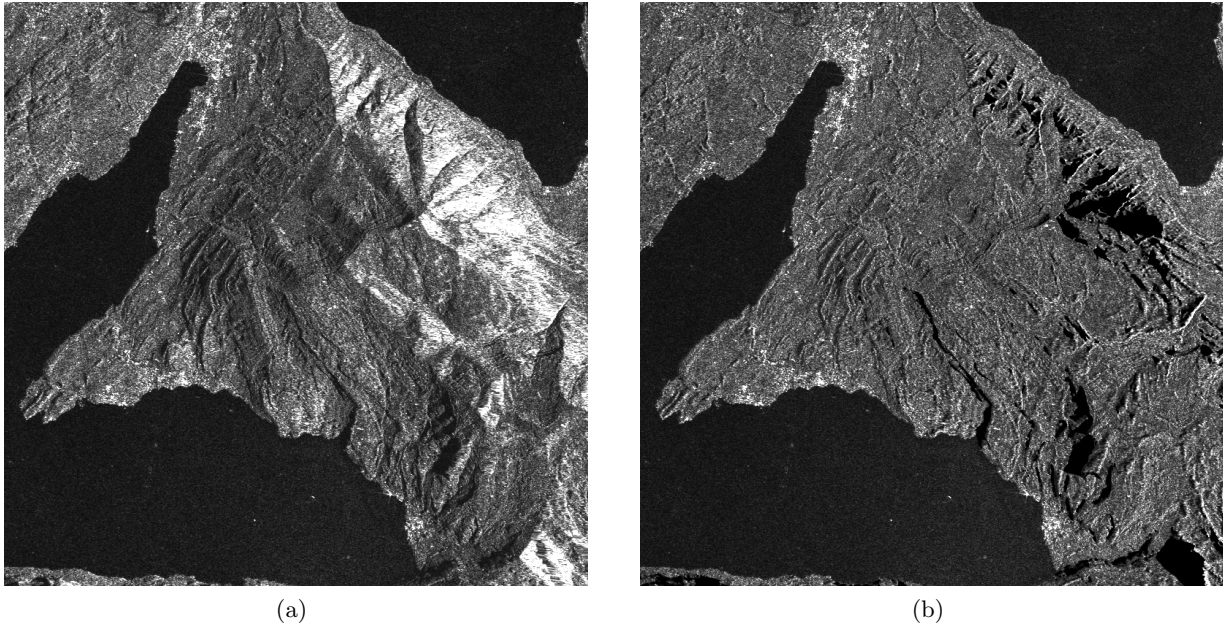


**Figure 2.** ENVISAT/ASAR IM image, descending orbit 7963, beam IS6 of Rigi Mountain in local map coordinates (Easting/Northing). (a) No radiometric correction. (b) Radiometric correction applying a stringent terrain-based elevation antenna gain pattern correction, and a correction for terrain slope induced variation of radar brightness. Layover and shadow regions are masked.

antenna gain pattern correction factors were calculated and multiplied by the backscatter coefficients at the corresponding image positions. A map of both slope correction and elevation antenna gain pattern correction factors at the central azimuth position are shown in Fig. 4. (Note that only the image positions which lie within the azimuth beam width get a contribution from a radar echo of a specific sensor position. A feature not shown in Fig. 4 but implemented in the TDBP algorithm.) The intensity distribution of the correction factors (Fig. 4(a)) coincides well with the backscatter coefficients of the radiometrically uncorrected SAR image (Fig. 2(a)).

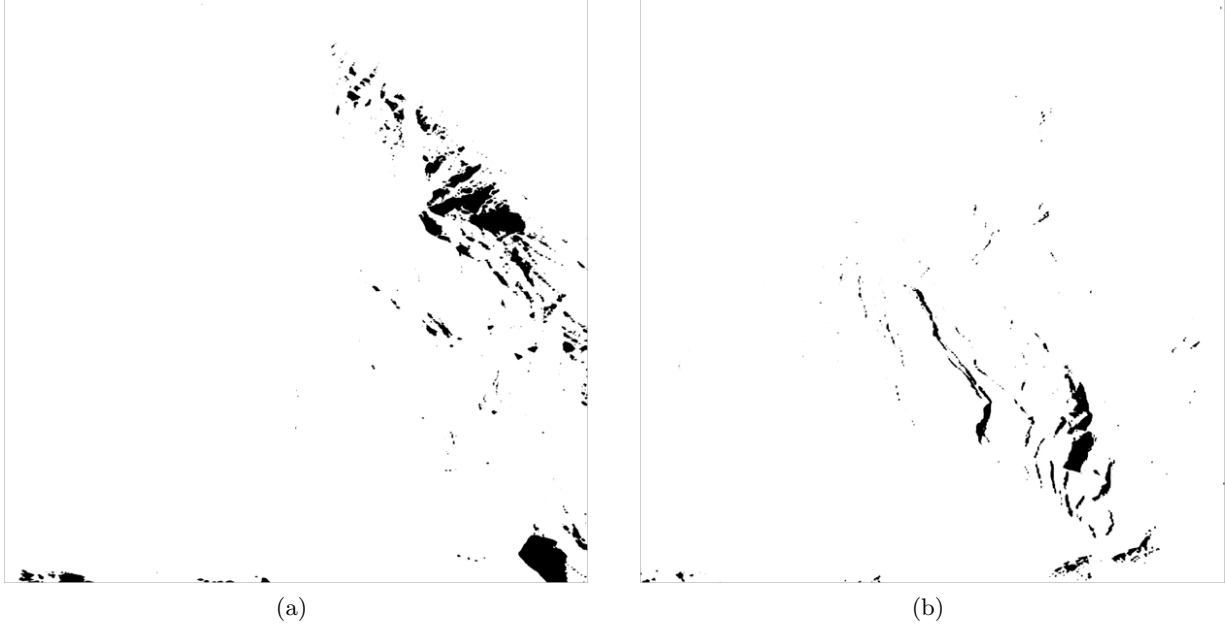
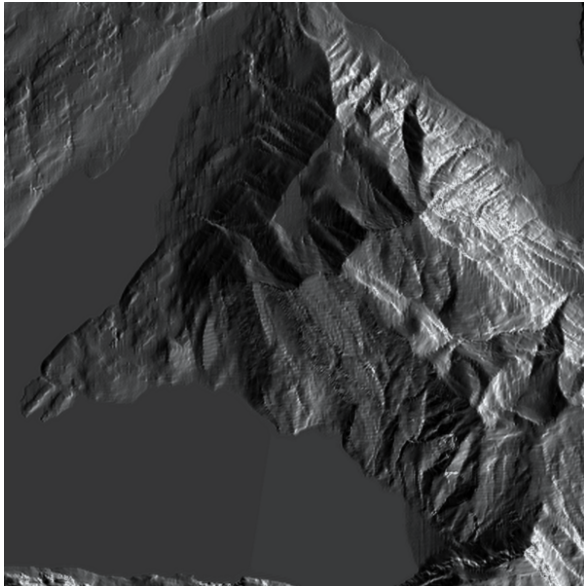


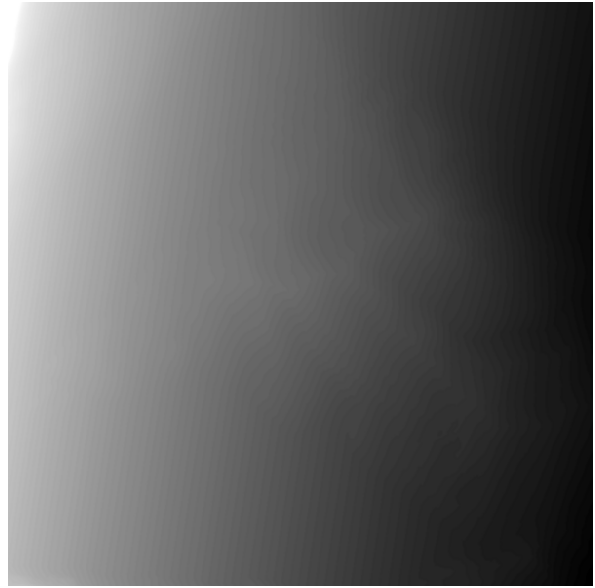
**Figure 3.** (a) Layover mask. (b) Shadow mask.

The effectiveness of the radiometric correction is validated by verifying the dependence of the average backscatter coefficient on the local incidence angle. In Fig. 5(a) this relationship is depicted. The data have been reorganised and subdivided according to classes of local incidence angles. All class intervals are of identical size – this implies that the number of elements per class depends on the frequency distribution of the local incidence angles occurring in the SAR scene under inspection. The averaged backscatter coefficient of each class is plotted against the corresponding local incidence angle. Layover and shadow regions have previously been excluded.

The deep notches that occur around  $\theta_l \approx 41^\circ$  in both of the graphs are caused by the fact that a considerable proportion of the scene consists of radar returns from the two lakes: as the water surface is relatively smooth in the SAR scene at hand the energy that is scattered back to the antenna is much lower than the energy that returns from a usually rougher land surface at the same local incidence angle. Therefore, the average backscatter coefficient is much reduced at this local incidence angle. In Fig. 5(b) the pixel locations at local incidence angles  $\theta_l \in [40^\circ, 41.5^\circ]$  are mapped, clearly showing the virtual congruence with the lake area. The uncorrected data in Fig. 5(a) show a strong dependence of the average backscatter coefficient on the local incidence angle: as expected the average backscatter coefficient is highest for small local incidence angles and the curve drops off for increasing local incidence angles. For local incidence angles  $\theta_l \in [20^\circ, 73^\circ]$  the radiometric correction removes this dependence to a large extent, the remaining variation being less than 1 dB – except the notch caused by the lakes. Within the same interval the uncorrected average backscatter coefficients span a range of more than 5 dB. However, backscatter coefficients corresponding to low and high local incidence angles tend to be underestimated. Especially for low local incidence angles the applied correction approach based on the projection cosine does not seem to be sufficient. Recall that it does not consider layover and shadow regions. But besides the approximative character of the radiometric correction, several reasons, which could explain the decrease of the curve for extreme local incidence angles, come into consideration. Inaccuracies in the digital elevation model lead to incorrect positioning and therefore wrong assignment of radiometric correction factors particularly in case of rugged terrain. In addition, the assumption of constant average backscatter coefficients for all local incidence angles is only valid for large and relatively homogeneous scenes – as exemplified by the dramatic influence of low backscatter from the lake surface. The terrain may exhibit slope-dependent surface texture characteristics. Finally, the number of elements per class, which provide the basis for the estimate of the average backscatter coefficient, decreases for extreme local incidence angles.

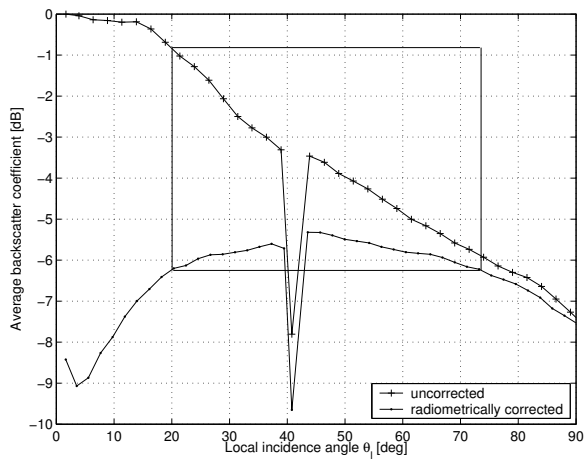


(a)

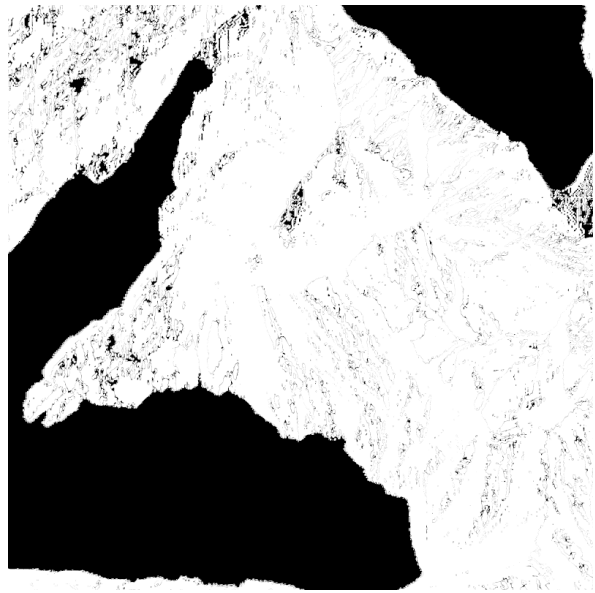


(b)

**Figure 4.** (a) Radiometric slope correction factors (projection cosine approach) and (b) stringent, DEM-based elevation antenna gain pattern correction factors at the central azimuth position mapped to the image grid in local map coordinates (Easting/Northing).



(a)



(b)

**Figure 5.** (a) Dependence of average backscatter coefficient on local incidence angle. Layover and shadow regions are excluded. (b) Black: map of local incidence angles  $\theta_l \in [40^\circ, 41.5^\circ]$ . The dependence of the average backscatter coefficient on the local incidence angle is well reduced (variation  $< 1$  dB) within  $\theta_l \in [20^\circ, 73^\circ]$  for the radiometrically corrected data. The low radar returns from the lake surface, all at local incidence angles between  $40^\circ$  and  $41.5^\circ$  (b), explain the notches in the graphs of (a).

The validation presented here has been restricted to the performance of the radiometric correction. However, the geolocation accuracy of ENVISAT/ASAR IM data processed by TDBP has already been assessed with the help of a corner reflector [8]. It was found that the geolocation error is below sample spacing in both range and azimuth.

## 7. CONCLUSIONS

An experimental framework based on time-domain back-projection processing for simultaneous azimuth focusing, geocoding and radiometric correction of SAR data of rugged terrain has been presented and tested with ENVISAT/ASAR image mode data. Currently, a projection cosine term is used in order to remove the terrain-induced variation of radar brightness. In addition, a stringent, terrain-based correction for the elevation antenna gain pattern is included.

An evaluation of the algorithm with respect to its ability to remove radiometric distortions caused by topography showed that for local incidence angles between  $20^\circ$  and  $73^\circ$  the correction reduces the variation of the averaged backscatter coefficient from originally more than 5 dB to less than 1 dB. For local incidence angles outside this interval, however, the correction is not satisfactory.

In order to improve the radiometric calibration more elaborate models have to be investigated in conjunction with the time-domain back-projection algorithm. When considering an extension of the method towards airborne SAR, in particular wide-beam systems, a more stringent terrain correction such as a facet-based estimation of local illuminated area seems to be indispensable. It is assumed that for such systems the benefit of time-domain back-projection processing even increases, because accurate reconstruction of the acquisition geometry and its relation to the terrain is more critical.

## ACKNOWLEDGMENTS

The authors would like to thank the European Space Agency for supplying the data and swisstopo for granting permission to use the DHM25 digital elevation model.

## REFERENCES

1. J. C. Curlander and R. N. McDonough, *Synthetic Aperture Radar - Systems and Signal Processing*, John Wiley & Sons, New York, 1991.
2. R. K. Raney, H. Runge, R. Bamler, I. G. Cumming, and F. Wong, "Precision SAR Processing Using Chirp Scaling," *IEEE Transactions on Geoscience and Remote Sensing* **32**(4), pp. 786–799, 1994.
3. A. Moreira and Y. Huang, "Airborne SAR Processing of Highly Squinted Data Using a Chirp Scaling Approach with Integrated Motion Compensation," *IEEE Transactions on Geoscience and Remote Sensing* **32**(5), pp. 1029–1040, 1994.
4. C. Cafforio, C. Prati, and F. Rocca, "SAR Data Focusing Using Seismic Migration Techniques," *IEEE Transactions on Aerospace and Electronic Systems* **27**(2), pp. 194–207, 1991.
5. I. G. Cumming and F. H. Wong, *Digital Processing of Synthetic Aperture Radar Data: Algorithms and Implementation*, Artech House Inc., Boston, London, 2005.
6. L. M. H. Ulander, H. Hellsten, and G. Stenström, "Synthetic-Aperture Radar Processing Using Fast Factorized Back-Projection," *IEEE Transactions on Aerospace and Electronic Systems* **39**, pp. 760–776, July 2003.
7. M. Soumekh, *Synthetic Aperture Radar Signal Processing: with MATLAB Algorithms*, John Wiley & Sons, 1999.
8. O. Frey, E. Meier, and D. Nüesch, "A Study on Integrated SAR Processing and Geocoding by Means of Time-Domain Backprojection," in *Proceedings of the Int. Radar Symposium, Berlin*, 2005.
9. D. Small, B. Rosich, A. Schubert, E. Meier, and D. Nüesch, "Geometric Validation of Low and High-Resolution ASAR Imagery," in *Proc. of the 2004 Envisat & ERS Symposium, ESA SP-572*, (Salzburg), Sep. 2004.
10. F. Holecz, A. Freeman, and J. van Zyl, "Topographic effects on the antenna gain pattern correction," in *IGARSS '95, Geoscience and Remote Sensing Symposium*, **1**, pp. 587–589, 1995.
11. O. Frey, E. Meier, D. Nüesch, and A. Roth, "Geometric Error Budget Analysis for TerraSAR-X," in *Proc. of EUSAR 2004 - 5th European Conference on Synthetic Aperture Radar*, pp. 513–516, (Ulm, Germany), May 25-27 2004.
12. D. Small, M. Jehle, E. Meier, and D. Nüesch, "Radiometric Terrain Correction Incorporating Local Antenna Gain," in *Proc. of EUSAR 2004 - 5th European Conference on Synthetic Aperture Radar*, pp. 929–932, (Ulm, Germany), May 25-27 2004.
13. J.-S. Lee, D. Schuler, and T. Ainsworth, "Polarimetric SAR data compensation for terrain azimuth slope," *IEEE Transactions on Geoscience and Remote Sensing* **38**(5), pp. 2153–2163, 2000.
14. L. M. H. Ulander, "Radiometric slope correction of synthetic-aperture radar images," *IEEE Transactions on Geoscience and Remote Sensing* **34**(5), pp. 1115–1122, 1996.
15. D. Small, F. Holecz, E. Meier, and D. Nüesch, "Absolute radiometric correction in rugged terrain: A plea for integrated radar brightness," in *IGARSS '98, International Geoscience and Remote Sensing Symposium*, **1**, pp. 330–332, 1998.
16. M. Otten and H. Boomkamp, "Estimation of the Absolute Orbit Accuracy of Envisat," tech. rep., European Space Operations Centre (ESOC), Robert-Bosch Strasse 5, D-64283 Darmstadt, 2003.